



## Present Limits on the Precision of SM Predictions in Signatures with Jets

The CDF Collaboration  
URL <http://www-cdf.fnal.gov>  
(Dated: February 21, 2010)

We evaluate the impact of theoretical uncertainties on the measured energy of hadronic jets. The analysis is performed using events with a  $Z$  boson and a single jet observed in  $p\bar{p}$  collisions at  $\sqrt{s} = 1.96$  TeV in  $4.62 \text{ fb}^{-1}$  of data from the Collider Detector at Fermilab (CDF). The jets are measured using the CDF non-compensating sampling calorimeters which have a non-linear response to single particles. The transverse momenta ( $p_T$ ) of the jet and the boson should balance each other due to momentum conservation in the plane transverse to the direction of the  $p$  and  $\bar{p}$  beams. We evaluate the dependence of the measured  $p_T$ -balance on theoretical uncertainties associated with initial and final state radiation, choice of renormalization and factorization scales, parton distribution functions, jet-parton matching, calculations of matrix elements, and parton showering. We find that the uncertainty caused by parton showering at large angles is largest. We conclude that special actions have to be taken to achieve an uncertainty on the jet energy scale of even 3% in an experiment with a non-linear hadronic calorimeter such as those at CDF and at the LHC, a possible limitation on discovery potential in signatures containing jets.

*Preliminary Results for Spring 2010 Conferences*

Contacts: A. Paramonov <paramon@hep.uchicago.edu>, H. Frisch <frisch@hep.uchicago.edu>, F. Canelli <canelli@hep.uchicago.edu>, M. D'Onofrio <donofrio@fnal.gov>, and S. Mrenna <mrenna@fnal.gov>

## I. STATEMENT OF THE PROBLEM IN SETTING THE JET ENERGY SCALE

The discovery potential of the LHC will strongly depend on the accuracy of Standard Model (SM) predictions, as any new physics has to be clearly separated from SM phenomena. In this paper we study the precision of modeling of the QCD jets that are produced in the majority of SM events. The uncertainties of the jet-related predictions directly impact the measurement of jet energies (jet energy scale, JES), missing transverse momentum, and, consequently, the discovery potential for supersymmetry and many other models of physics beyond the SM [1]. This is especially important for experiments which use non-compensating calorimeters such as CMS, ATLAS, and CDF [2]. The impact on the discovery potential depends on the detector technology, jet clustering, and event selection.

It has been a common practice to relate a clustered jet energy, measured in a calorimeter, to energy of the particle jet or the parent parton [3, 4]. The relation is performed by correcting the measured jet energy for instrumental effects, and fragmentation and radiation effects. Some of the corrections can not be extracted from data so that one relies on the accuracy of the SM predictions. Some of the uncertainties on the predictions are estimated by varying parameters of the ingredient models. However, the ingredient models do not work well across the whole phase-space of transverse momentum and separation of jets; one has to estimate the uncertainties due to the limited coverage of the phase space separately. The latter set of uncertainties can be estimated by comparing predictions to data. In the end, the total uncertainty on the jet energy corrections can be disentangled into individual components, which need to be combined into the total uncertainty.

We take events with a  $Z$  boson and a jet observed in  $p\bar{p}$  collisions at  $\sqrt{s} = 1.96$  TeV in  $4.62 \text{ fb}^{-1}$  of data from CDF as a precision SM process to test the measured jet energy using  $p_T$ -balance,  $p_T(\text{jet})/p_T(Z)$  (see Section II). The  $Z$  bosons are observed as clearly-identified pairs of electrons or muons. The transverse momentum of the bosons is also well-measured making them an ideal instrument for the analysis. We find that the observed  $p_T$ -balance is different from that given by the predictions. The overall discrepancy between the observed and the predicted balances was previously used to estimate the uncertainty on the JES at CDF [3]. In this paper we investigate the sources of uncertainties contributing to the observed discrepancy and the precision of the SM predictions for hadronic jets. Finally, we compare the total of the uncertainties and the observed discrepancy to check the completeness of the investigation.

The JES at CDF is determined independently of the  $p_T$ -balance using the measured single particle response in the calorimeters [3]. The in-cone (see Section III B) parton showering (PS) has been extensively studied [5, 6] and is in a good agreement with the predictions. We rely on the predicted energy of the leading (highest in  $p_T$ ) jet to study the  $p_T$ -balance in  $Z$ -jet events.

Predictions at higher energies are based on a simplified modeling of complex SM processes in the simulation event generators [7, 8]. The complex event models are built of simpler sub-models that can be altered by tuning parameters of the generator. The list of uncertain parameters and sub-models we investigate includes:

- Parton distribution functions (PDF's) of the colliding  $p$  and  $\bar{p}$ ,
- Matrix elements of the tree-level processes such as  $q\bar{q} \rightarrow Zg$  and  $qg \rightarrow Zq$ ,
- Parton-jet matching scheme [9],
- Final state radiation (FSR) parameters of PYTHIA,
- Initial state radiation (ISR) parameters of PYTHIA,
- The  $Q^2$  scale multiplier parameter of ALPGEN.

In addition to that we investigate uncertainties due to multiple  $p\bar{p}$  interactions and the limited ability of the parton showering (fragmentation) model to describe FSR at large angles.

We demonstrate that the uncertainty due to large-angle final state radiation is significant and is comparable to the disagreement between data and SM predictions. The other uncertainties are on the order of 1-2% and are smaller than the observed discrepancy.

Additional improvements in the description of SM QCD processes are required to improve the discovery potential of the LHC experiments. Having the large-angle FSR as one of the largest sources of discrepancy dictates a need for higher-order corrections to the parton showering or a parton-jet matching scheme which would cover the problematic region [10].

## II. THE ANALYSIS STRATEGY

We evaluate the limitations of the Standard Model (SM) predictions from PYTHIA by studying events with a  $Z$ -boson balancing against a jet. For each event with a single jet back-to-back in  $\vec{p}_T$  to a  $Z$ -boson we compare the  $p_T$  of the leading (highest- $p_T$ ) jet to that of a  $Z$ -boson by calculating a  $p_T$ -ratio,  $p_T(\text{jet1})/p_T(Z)$ . The  $p_T$ -ratios are compared between data and SM predictions in events as a function of  $p_T(Z)$ . The accuracy of the approach relies on well-measured and well-understood quantities such as the transverse momenta of the  $Z$ -boson and the jet.

We use the  $p_T$ -ratios to investigate the out-of-cone energy of jets, kinematical properties of  $Z$ -jet events, and other theoretical uncertainties of SM QCD predictions. These measurements are uniquely possible in CDF since the JES [3] was calibrated via tuning of the calorimeter response of single particles, rather than using  $p_T$ -balance as is often used elsewhere. In addition, the momentum spectra of charged-particle tracks in jets are found to be in good agreement with SM predictions [3]. The test of  $p_T$ -balance in  $Z$ -jet events is consequently independent of the standard CDF JES calibration.

The  $Z$ -jet system is not a perfect two-body process and the  $p_T$ -balance is sensitive to the surroundings of the jet. Also, the jet energy resolution is rather poor (comparable to the jet energy) for jets with  $p_T$  of about 10 GeV/ $c$ . The resolution improves with higher jet energies. To approach the ideal two-body system we apply exclusive event selection which is not used for regular physics analysis. We select events with  $p_T(Z) > 25$  GeV/ $c$  to avoid the effect due to the jet energy resolution. In addition,  $p_T$  of sub-leading jets is required to be less than 3 GeV/ $c$  to suppress FSR. The  $p_T$ -balance for the exclusive event selection is shown in Fig. 1 (b); the both distributions average close to 1.0. Absence of  $p_T(Z) > 25$  GeV/ $c$  requirement spoils the distribution as shown in Fig. 1 (a). Changing the 3 GeV/ $c$  cut-off on the  $p_T$  of sub-leading jets to 8 GeV/ $c$  introduces additional discrepancy between data and SM predictions as shown in Figs. 4, 5, and 6.

We observe a discrepancy between the  $p_T$ -balance in data and that predicted with event generators (see Figs. 4, 5, and 6). We investigate the discrepancy by studying the quark-gluon composition of the leading jet and the momentum carried by the sub-leading jets. In addition we evaluate changes of the predicted  $p_T$ -balance by altering parameters of the event generators (ALPGEN and PYTHIA).

The initial hypothesis was that the discrepancies were due to incorrect fractions of quark and gluon jets in the predictions (quark and gluon jets deposit different energies in the CDF calorimeter). We check the ratios of quark and gluon jets directly using tracks in the jet cone; we observe good agreement. We evaluate the dependence of the  $p_T$ -balance on variations of parameters in PYTHIA and ALPGEN MC generators. We vary the rates of Final State Radiation (FSR) and Initial State Radiation (ISR),  $Q^2$ -scale multipliers, and Parton Distribution Functions (PDF's). We find that none of those uncertainties are as large as the observed discrepancy between data and the SM predictions.

We have also investigated the energy flow outside the cone of the leading jet using the sub-leading (2nd highest in  $p_T$ ) jet. We observe a higher rate of sub-leading jets collinear to the leading jet in data than in the predictions. We show that the large-angle radiation observed as the sub-leading jets can explain the discrepancy between data and MC.

## III. EVENT SELECTION

The analysis uses events selected by the trigger system that contain either a central electron with  $E_T > 18$  GeV or a muon with  $p_T > 18$  GeV/ $c$  [11]. The electron dataset contains 229M events; the muon dataset contains about 65M events. The integrated luminosity of each dataset is 4.62 fb $^{-1}$ .

Both the observed and the simulated events (see Section IV) are processed through the same selection criteria to identify electrons and muons, jets, and  $Z$  bosons. Details of the selection criteria are

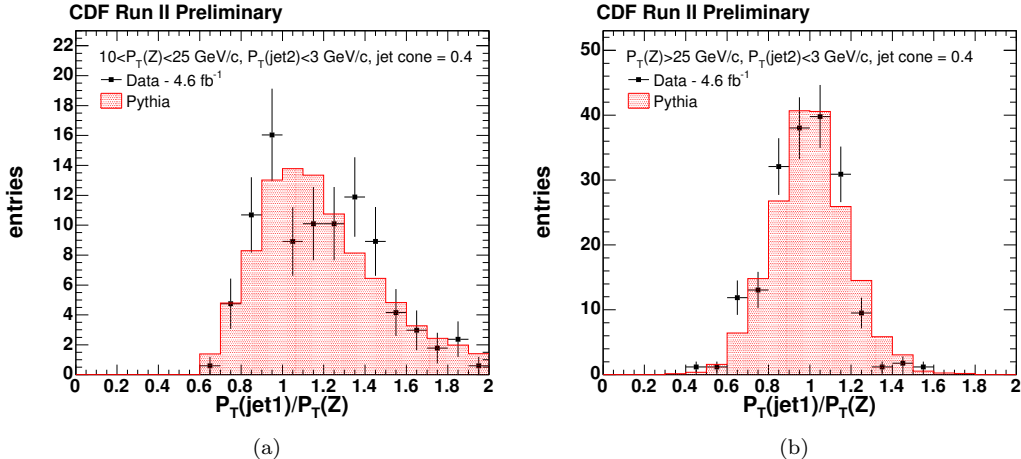


FIG. 1: The observed (points) and expected (histogram) distributions in  $p_T$ -balance,  $p_T(\text{jet})/p_T(Z)$ , for events with  $p_T(Z)$  less than 25 GeV/ $c$  (Fig. a) and greater than 25 GeV/ $c$  (Fig. b). Sub-leading jets are required to have  $p_T < 3$  GeV/ $c$  to suppress energy flow outside of the cone of the leading jet (see Section III B). The distribution (a), for  $p_T(Z) < 25$  GeV/ $c$ , is noticeably distorted from a symmetric Gaussian shape due to a finite jet energy resolution and a cut-off on the minimum  $p_T$  of the leading jet. The predicted distributions are produced with the PYTHIA MC event generator.

provided in Appendix B.

### A. The CDF II detector

The CDF Run II detector is described in detail in Appendix A. The CDF hadronic calorimeters have steel-scintillator sampling design and the electromagnetic calorimeters are build of lead and scintillator. The sampling calorimeters have a non-linear response to stable hadrons [3], which carry the most of jet momentum.

### B. Jet identification

Jets are reconstructed using the standard CDF cone-based clustering algorithm with cone radii of 0.4, 0.7, and 1.0 [12]. The clustering is performed using calorimeter towers with raw, uncorrected, energy above 1 GeV to form a cluster of at least 3 GeV.

The jet energies are corrected for the  $\eta$ -dependent response of the calorimeters and for the luminosity-dependent effect of multiple- $p\bar{p}$  interactions. The simulated calorimeter response for individual hadrons is tuned to match that in data [3]. Then the leading jet energy is corrected to the parton level; the absolute (hadron) jet energy scale is adjusted to relate the measured energy of a simulated jet and the energy of the corresponding parton in di-jet events [3]. The correction from the hadron to the parton level is a function only of  $p_T$  of a jet and it is the same for data and predictions.

Calorimeter clusters that coincide with an identified electron, or photon are removed; i.e. each calorimeter cluster can be associated with either a jet, an electron, or a photon, which have mutually exclusive definitions to avoid any ambiguities. Also we remove events where the leading jet coincide with one of the muons forming a  $Z$  boson.

The vertex of origin of a jet is determined using tracks pointing to the towers in the jet cluster. The tracks are extrapolated to the beam-line where we take the  $z$ -coordinate for each track at the point closest to the beam-line ( $z_0$ ). We combine the measured  $z_0$  values for all tracks associated to the jet

weighted with their uncertainties to form the average value for the jet. The root mean square is also calculated using the  $z_0$  values.

We remove events where the leading jet is unrelated to the production of the  $Z$ -boson using the jet vertex of origin. We require the jet vertex or origin to be consistent with the primary vertex of the lepton pair forming the boson. The rejection procedure removes events where the leading jet has two or more tracks and its vertex of origin is more than 2 cm away from the vertex of the lepton pair.

High- $p_T$  photons are not rare in hard-scattering events. Identifying photons as jets and then correcting them as jets can lead to mis-measured  $p_T$ -balance. To avoid the photon candidates we require the leading jet to have EM-fraction less than 0.95. The EM-fraction is the fraction of energy of a jet deposited in the electromagnetic compartment of the calorimeter in comparison to the total energy of the jet.

### C. Selection of $Z$ +jet events

To be identified as a  $Z$  boson a pair of opposite-sign electrons or muons must have a reconstructed invariant mass in the mass window from 80  $\text{GeV}/c^2$  to 100  $\text{GeV}/c^2$ . The selection of  $Z \rightarrow \ell\ell$  events requires two tight leptons or a tight and a loose lepton. The two leptons are required to be assigned the same primary vertex. Figure 2 shows the distributions in invariant mass for electron and muon pairs.

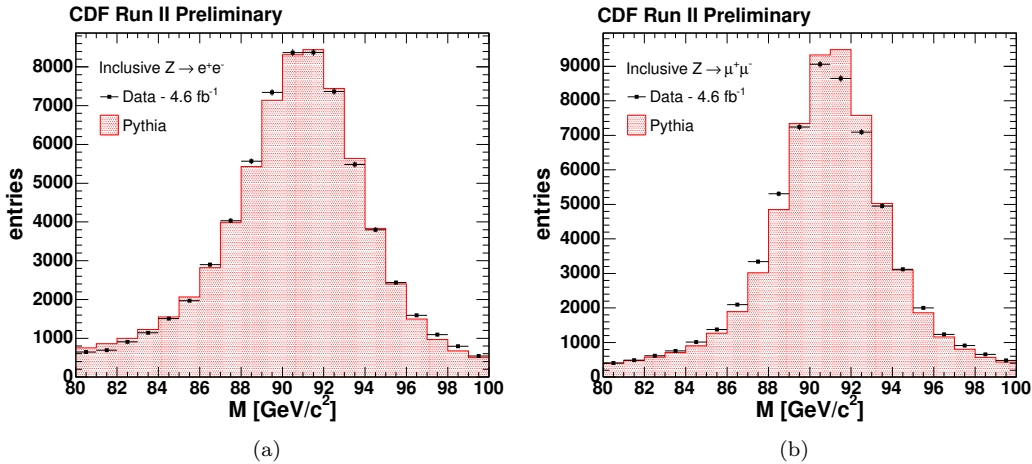


FIG. 2: The observed (points) and expected (histogram) distributions in the invariant mass of  $e^+e^-$  (Fig. a.) and  $\mu^+\mu^-$  (Fig. b.) lepton pairs.

First, we correct energies of the all jets for  $\eta$ -dependent effects of the calorimeter and for multiple  $p\bar{p}$ -interaction. Then we require the leading jet's  $p_T$  to be greater than 8  $\text{GeV}/c$  when the sub-leading jet's  $p_T$  is always less than 8  $\text{GeV}/c$  ( $|\eta|$  of a jet can be up to 2.8). Leading jet's absolute value of detector  $\eta$  is required to be from 0.2 up to 0.8,  $0.2 < |\eta_{\text{det.}}| < 0.8$ , to avoid cracks in the central calorimeter. The fraction of the measured electromagnetic energy of the leading jet has to be greater than 0.95. We do not apply the latter two cut-offs to the sub-leading jet. The  $\vec{p}_T$  of the leading jet ( $\vec{p}_T(\text{jet1})$ ) and the  $\vec{p}_T$  of the  $Z$  boson ( $\vec{p}_T(Z)$ ) are required to be back to back:  $\Delta\phi(\vec{p}_T(\text{jet1}), \vec{p}_T(Z)) > 3.0$  rad. Finally, we correct the energy of the leading jet to match that of the parent parton [3]; the correction is not applied to sub-leading jets.

We test precision of the measurement of  $p_T(Z)$  by using simulated events. In each event we find the observed  $p_T(Z)$  to within 0.5% of the generated value. A distribution of the observed transverse momentum of  $Z$ -bosons,  $p_T(Z)$ , is shown in Fig. 3.

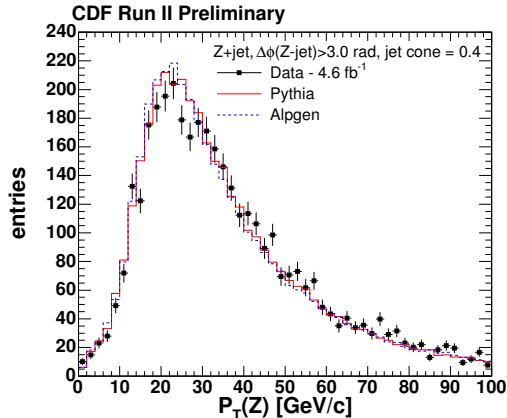


FIG. 3: The observed (points) and expected (histogram) distributions in the transverse momentum of lepton pairs with invariant mass between  $80 < M(\ell\ell) < 100 \text{ GeV}/c^2$ . All other sample selection cuts have been applied.

#### IV. STANDARD MODEL PREDICTIONS OF EVENTS WITH A $Z$ BOSON AND JETS

The standard model expectations for the production of  $Z$  bosons are calculated from Monte Carlo simulations. We use PYTHIA and ALPGEN to generate  $Z$  + light jets processes.

The datasets for the  $Z$  + light jets signatures are produced using a version of PYTHIA customized by CDF in which the  $p_T$  spectrum of the  $Z$  bosons,  $p_T^Z$ , has been tuned to CDF Run I data for  $0 < p_T^Z < 20 \text{ GeV}/c$ , and which incorporates a tuned underlying-event [13] and a requirement that  $M_{\text{inv}}(\ell\ell) > 30 \text{ GeV}/c^2$ . The event generator was set to inclusive production of  $Z$ -bosons.

Additional  $Z$  + jets samples are produced with a version of ALPGEN that has built-in matching of the number of jets from showering and matrix-element production [14]. The exclusive  $Z$  +  $N$  partons ( $N=0,\dots,4$ ) samples were combined into one using the corresponding cross-sections provided by ALPGEN. Showering and hadronization of jets is done with PYTHIA [15]. The jet-parton matching was performed at  $15 \text{ GeV}/c$  using jet cone of 0.4. Events from the MC generators, ALPGEN and PYTHIA, are processed through the full detector simulation to be reconstructed and analyzed like data.

#### V. PROPERTIES OF QUARK AND GLUON JETS

Properties of a QCD jet depend on the tree-level parton initiating it. A jet initiated by a gluon has higher multiplicity of stable hadrons than a jet of the same energy initiated by a light quark. The difference in the observed particle multiplicities is due to the different color charges of a quark and a gluon. Similarly gluon jets produce a softer spectrum of stable hadrons than quark jets.

Quark and gluon jets of the same momentum deposit different amounts of energy in a non-compensating sampling calorimeter due to the non-linear response of the calorimeter to charged hadrons. On average quark jets produce more energy than gluon jets of the same true momentum. To illustrate that we show  $p_T$ -balance for quark and gluon jets in Figs. 4, 5, and 6. In this study we rely on the PYTHIA predictions for quark and gluon jets and on the well-tuned single particle response.

The fraction of quark and gluon jets in the  $Z$ -jet sample is largely driven by the parton distribution functions of the colliding particles (e.g.  $p\bar{p}$  at the Tevatron and  $pp$  at the LHC) and the matrix elements of  $q\bar{q} \rightarrow Zg$  and  $qg \rightarrow Zq$  tree-level diagrams.

We test a hypothesis that the data-predictions discrepancy of the  $p_T$ -balance is caused by the incorrectly predicted fraction of quark/gluon jets by using the number of tracks inside the jet cone

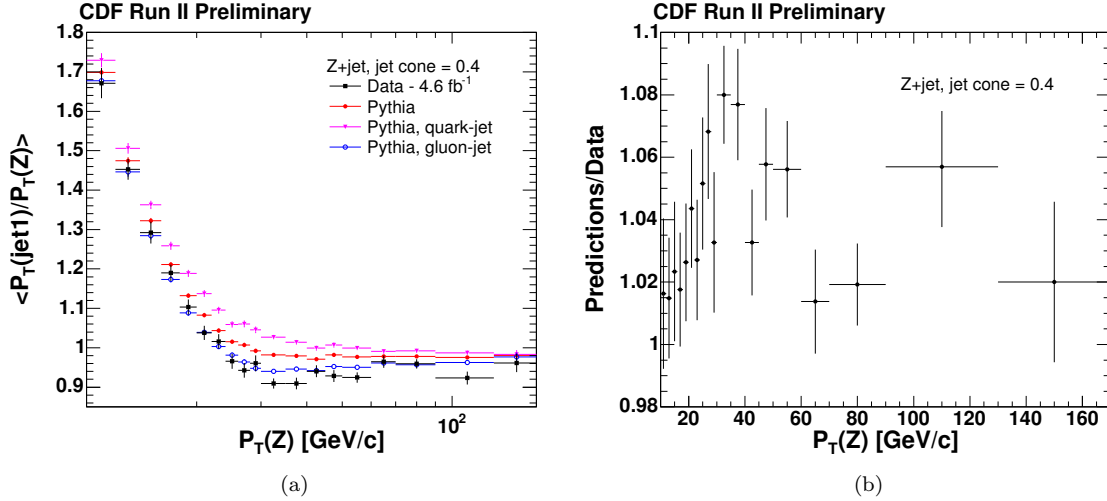


FIG. 4: a.) The average  $p_T$ -balance as a function of  $p_T(Z)$ . b.) The ratio of predicted and measured distributions in  $p_T$ -balance. The jets are clustered using a cone radius of 0.4.

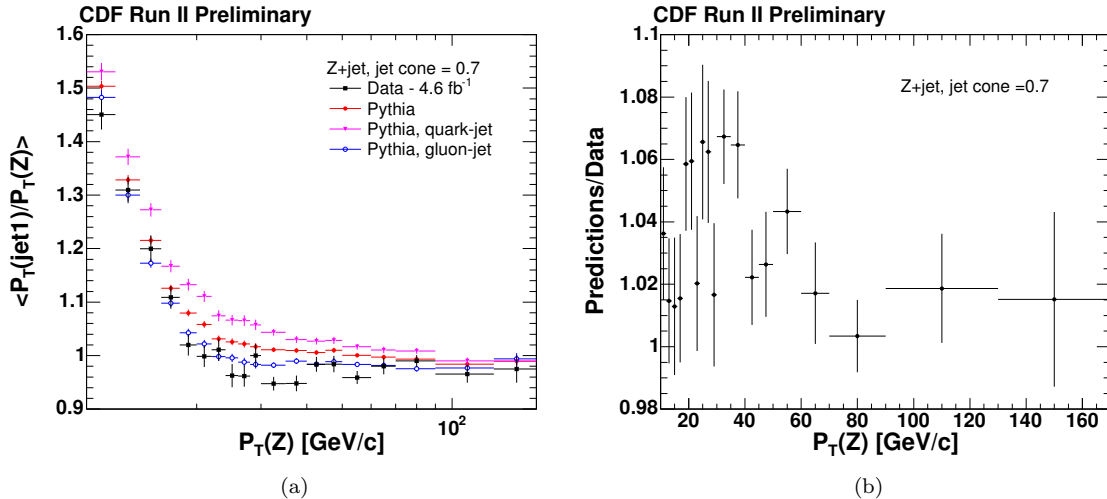


FIG. 5: a.) The average  $p_T$ -balance as a function of  $p_T(Z)$ . b.) The ratio of predicted and measured distributions in  $p_T$ -balance. The jets are clustered using a cone radius of 0.7.

(see Sec. VA) and rapidity distributions of  $Z$ -jet events (see Sec. VB). Both methods demonstrate good agreement between data and the SM predictions.

Also, we vary parameters of the event generators to estimate the dependence of the  $p_T$ -balance due to the uncertainty of the predicted fractions of quark/gluon jets. Variation of PDF's is described in Section VC and the matrix-element sensitive parameter are studied in Sections VC, VD, VE, and VF.

We exclude the hypothesis of the incorrect fraction of quark/gluon jets. The variations of the MC parameters are not sufficient to explain the observed discrepancy and the quark-gluon properties of data are in the agreement with the SM predictions.

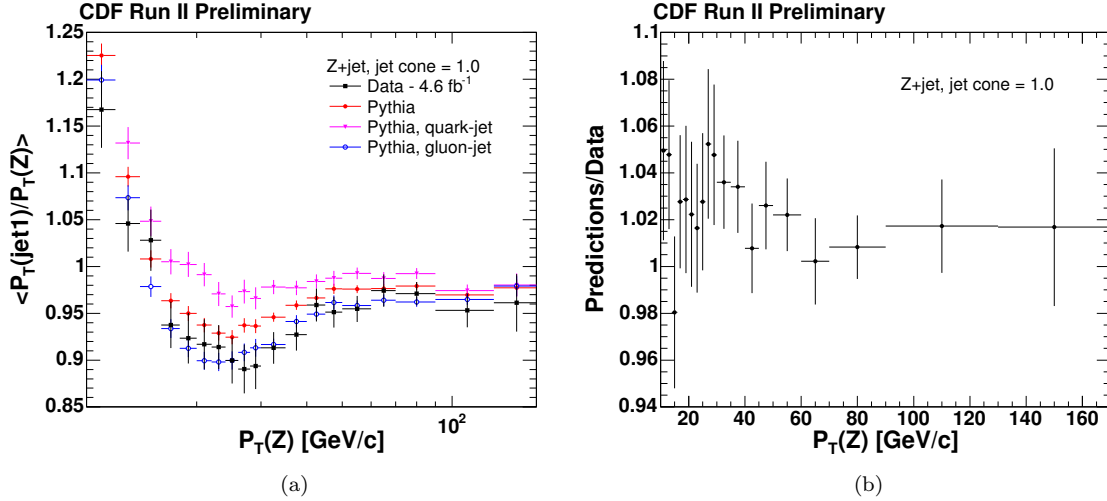


FIG. 6: a.) The average  $p_T$ -balance as a function of  $p_T(Z)$ . b.) The ratio of predicted and measured distributions in  $p_T$ -balance. The jets are clustered using a cone radius of 1.0.

### A. Charged particle multiplicity in jets

We perform a direct test of the quark-gluon composition of the observed jets by using the number of tracks observed within the jet cone. The number of tracks is different for quark and gluon jets (see Fig. 7, 8, and 9). Overall, the observed events are in a good agreement with the SM predictions (PYTHIA).

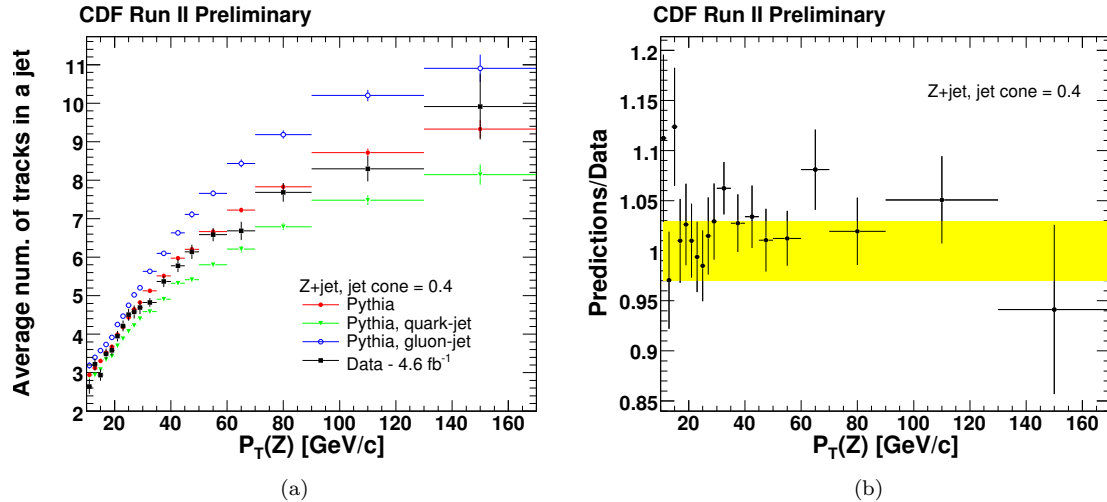


FIG. 7: a) The average number of tracks within a jet cone of radius of 0.4 as a function of  $p_T(Z)$ . b) The ratio of the predicted number of tracks to the measured number in data versus  $p_T(Z)$ . The yellow band represents a 3% uncertainty on the predicted tracking efficiency [16].

We calculate the number of tracks reconstructed within the cone of the leading jet. The tracks are required to originate from the same vertex as the lepton pair forming a  $Z$  boson,  $|z_0 - z_{\text{track}}| < 4$  cm

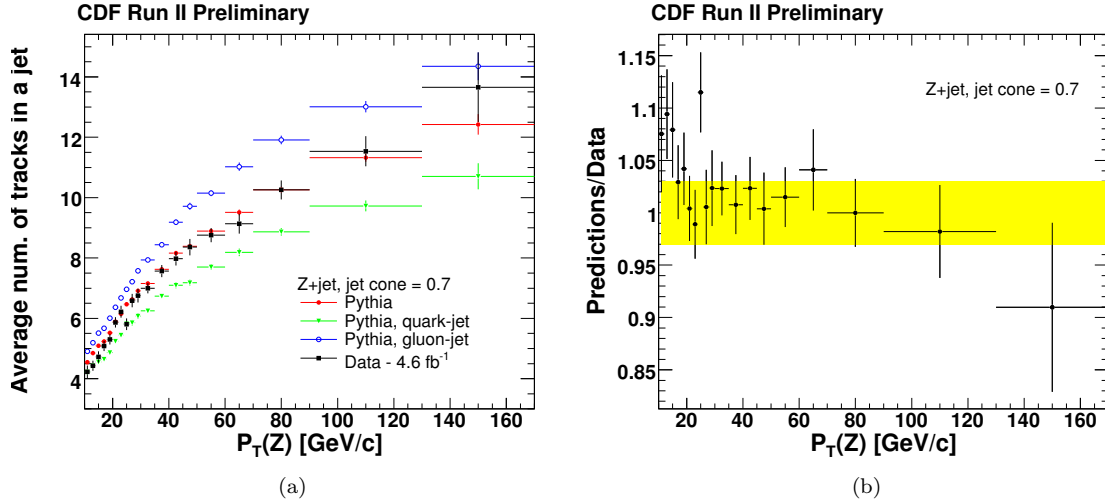


FIG. 8: a) The average number of tracks within a jet cone of radius of 0.7 as a function of  $p_T(Z)$ . b) The ratio of the predicted number of tracks to the measured number in data versus  $p_T(Z)$ . The yellow band represents a 3% uncertainty on the predicted tracking efficiency [16].

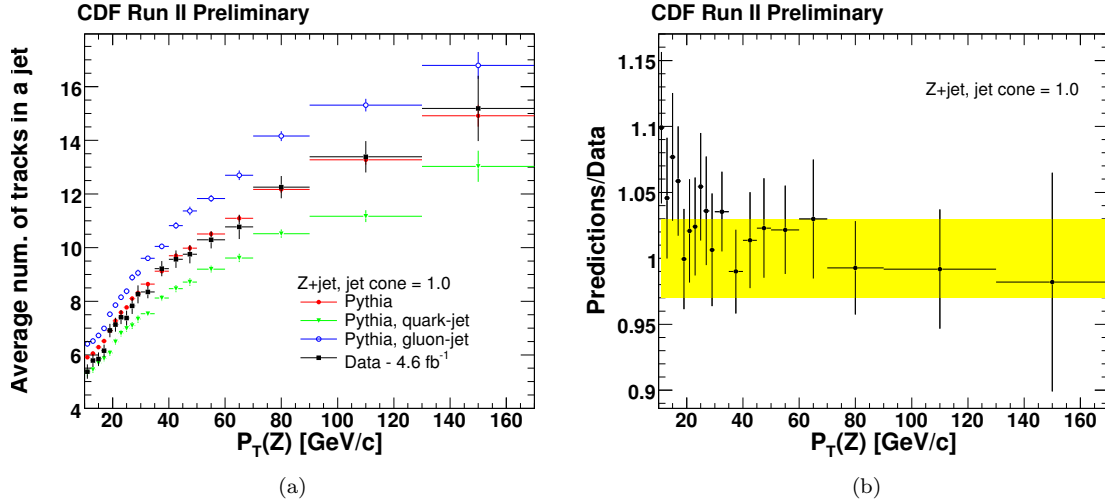


FIG. 9: a) The average number of tracks within a jet cone of radius of 1.0 as a function of  $p_T(Z)$ . b) The ratio of the predicted number of tracks to the measured number in data versus  $p_T(Z)$ . The yellow band represents a 3% uncertainty on the predicted tracking efficiency [16].

and  $|d_0(\text{tracks})| < 0.02$  cm (with SVX hits, 0.2 cm without SVX). Also we require good fit quality of the tracks,  $\chi^2/(\#\{COT\ hits\} - 5) < 6$ . Transverse momentum of the tracks is required to be greater than  $0.3$  GeV/c.

### B. Kinematic properties of $Z$ +jet events

Kinematical properties of  $Z$ +jet events and quark/gluon composition of the leading jet both depend on the PDF's and the matrix elements. Therefore, the kinematic properties probe indirectly the quark/gluon composition. The SM predictions are studied using the distributions of sum and difference of rapidities of a  $Z$  boson and the leading jet,  $|y(Z) + \eta(\text{jet1})|$  and  $|y(Z) - \eta(\text{jet1})|$ , respectively (see Fig. 10, 10, and 10). We require  $p_T(Z) > 15$  GeV/ $c$ . We observe good agreement between data and the predictions (both ALPGEN and PYTHIA).

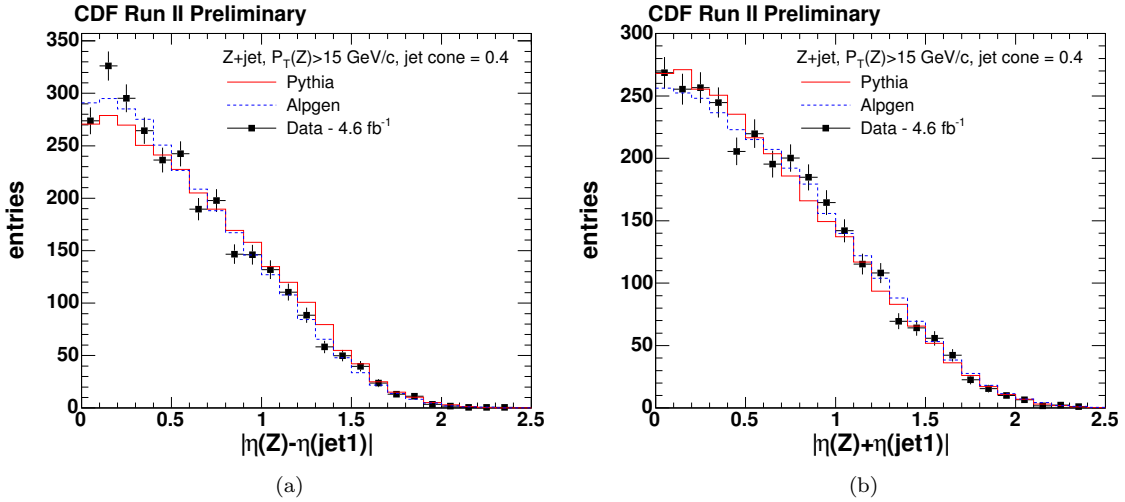


FIG. 10: The rapidity distributions for the  $Z$ +jet system. The jet clustering is performed with a cone of 0.4

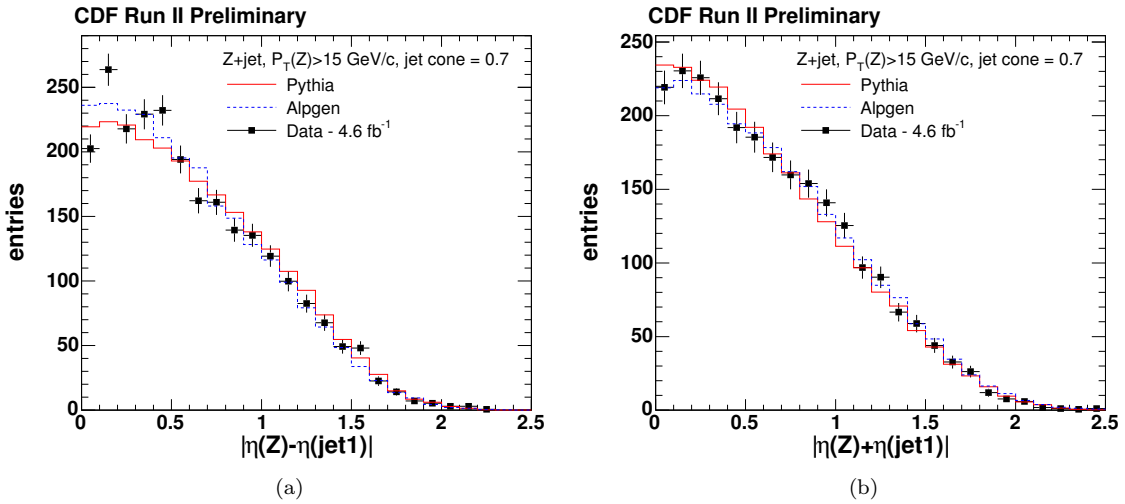


FIG. 11: The rapidity distributions for the  $Z$ +jet system. The jet clustering is performed with a cone of 0.7

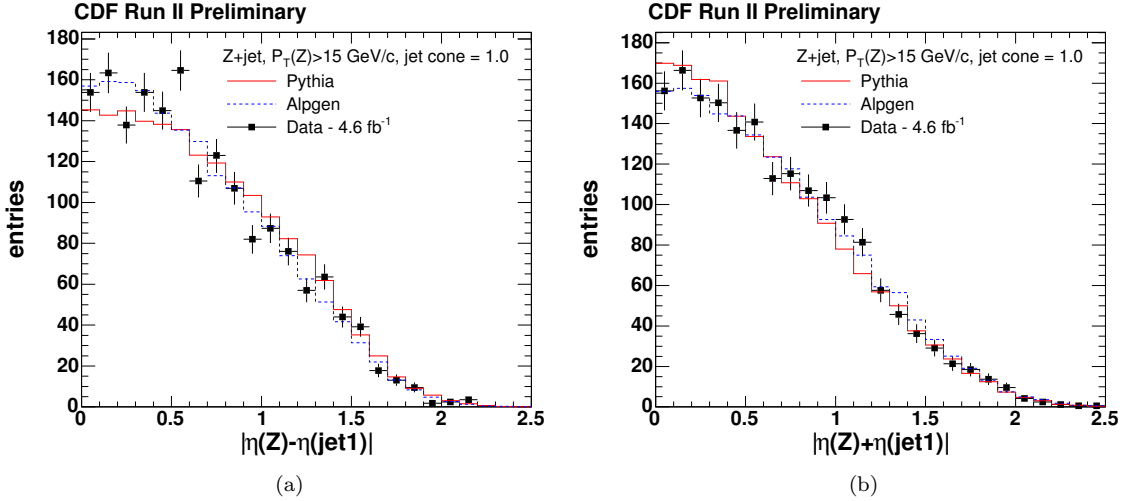


FIG. 12: The rapidity distributions for the  $Z$ +jet system. The jet clustering is performed with a cone of 1.0

### C. Dependence on PDF uncertainties

We test sensitivity of the  $p_T$ -balance on the choice of the PDF set used to generate events. The default PDF set, CTEQ5L, is a single set of functions and it does not contain error functions. To estimate the PDF-related systematic uncertainty we use CTEQ6M set, which includes 40 eigenvector error functions in addition to the central value. We re-weight the existing events using the parton densities provided by the CTEQ6M set. We calculate the difference in  $p_T$ -balance obtained for an error set relative to the central value given by CTEQ6M. The 40 variations in  $p_T$ -balance are added up in quadratures to obtain a negligibly small systematic uncertainty on the  $p_T$ -balance of about  $5 \cdot 10^{-3}$  %.

### D. Dependence on ISR uncertainties

In our Monte Carlo sample of inclusive  $Z$  events generated using PYTHIA, most of the jets arise from the ISR parton shower model (the underlying event model also contributes to jet production), which depends upon several parameters that are not tightly constrained by data. As a result, the parameters of ISR affect the observed  $p_T$ -balance in  $Z$ +jet events.

To produce the systematics samples we altered the ISR settings used in PYTHIA as described in Table I. Parameter MSTP(3) governs the choice of the  $\Lambda$  parameters used in the calculations of space-like (ISR) and time-like (FSR) parton showers. The parameter  $\Lambda$  is used in running of  $\alpha_s$ . By default when MSTP(3) is 2, the value of  $\Lambda$  is chosen according to the PDF parameterizations. We set MSTP(3) to 1 to overwrite the value of PARP(61), which defines  $\Lambda$  used in space-like parton showers. Parameter PARP(64) is also used in the calculation of  $\alpha_s$  and parton distributions as a multiplier for the squared transverse momentum evolution scale[43],  $k_{\perp}^2$ .

The  $p_T$ -balance obtained for the systematics samples is compared between the samples; the ISR-related variations of the  $p_T$ -balance are on the order of 1%.

Sample type	PARP(61), $\text{GeV}/c^2$	PARP(64)
default ISR	0.146	1.0
more ISR	0.292	0.5
less ISR	0.073	2.0

TABLE I: PYTHIA settings used to generate the samples for studies of the systematic uncertainties due to ISR. The input parameter MSTP(3) was set to 1 before providing these values to the event generator.

### E. Dependence on renormalization and factorization scales

Predictions for  $Z$ +jet production are sensitive to the choice factorization and renormalization scales. The scales impact calculation of the LO matrix elements for events with a  $Z$  boson and  $N$  partons.

We exploit ALPGEN to generate events with altered  $Q = qfac \times Q_0$  scales[44] (the renormalization and factorization scales are always kept the same by ALPGEN) by setting  $qfac = ktfac$  [45] to 0.5 or 2.0 simultaneously. The CDF default is  $qfac = ktfac=1.0$ . The choice of the scales impacts the predicted  $p_T$ -balance by up to 1-2%. The scale-related uncertainty of the  $p_T$ -balance is significantly smaller than the discrepancy observed between data and the SM predictions.

The choice of the scales in ALPGEN is similar to the ISR settings in PYTHIA for the inclusive production of  $Z$  bosons. The both of them impact calculation of the LO matrix elements. We are going to use the variation of  $p_T$ -balance given by the  $Q$ -scales in ALPGEN rather than ISR in PYTHIA to avoid double-counting of the effect.

### F. Dependence on the matrix elements and the jet matching scheme

Production of  $Z$ +jet events is performed differently by stand-alone PYTHIA and ALPGEN+PYTHIA. The ALPGEN+PYTHIA calculation begins with the exact matrix elements from ALPGEN for  $Z+N$  partons ( $N=0-4$ ), that are then interfaced with PYTHIA. The interface contains a veto algorithm that removes double-counting between matrix element and parton shower partons. The stand-alone PYTHIA calculation begins with the simplest matrix element ( $Z+0$  partons) and adds additional partons from the shower with no need for a veto. However, the first parton emission is corrected to reproduce the  $Z+1$  parton matrix element. Thus, any substantial differences between the two calculations (if they exist) should arise for the second jet. The both event generators use the same PDF set, CTEQ5L, and hadronization model.

We have compared  $p_T$ -balance in events produced with ALPGEN and PYTHIA. The difference between the event generators can be as high as 2-3%. We add it to the set of systematic uncertainties on the predicted  $p_T$ -balance.

## VI. CHARACTERISTICS OF OUT-OF-CONE RADIATION

An understanding of the energy flow outside of the leading jet's cone is essential for interpreting the measurement of  $p_T$ -balance in  $Z$ -jet events. Raw calorimeter energy summed in annuli outside of the jet cone requires a sophisticated treatment since the calorimeter response is especially non-linear for the softer particles. Also, the energy is sensitive to the pile-up of additional  $p\bar{p}$  interactions and the underlying event.

Instead of using the out-of-cone energy directly, we exploit correlations between  $p_T$ -balance and properties of the sub-leading jet (e.g.  $p_T$ ,  $\Delta\phi(jet1 - jet2)$ , etc.). Multiple in-time  $p\bar{p}$  interactions produce jets which are unrelated to the leading jet recoiling against the  $Z$ -boson. The presence of multiple interactions in an event diminishes the correlation between the  $p_T$ -balance and the properties of the sub-leading jet. In this section we require all events to have exactly one primary vertex to avoid the events with overlapping  $p\bar{p}$  interactions.

We measure the dependence of the  $p_T$ -balance on difference in  $\phi$ -angle between the leading jet ( $jet1$ ) and the sub-leading one ( $jet2$ ),  $\Delta\phi(jet1 - jet2)$ , for events with  $p_T(Z) > 25$  GeV/c (see Fig. 13, 14, and 15). The correlation depends on the jet cone size. The data is inconsistent with the predictions for jets with cone of 0.4 (see Fig. 13). This inconsistency indicates that the data has more large-angle radiation than the predictions.

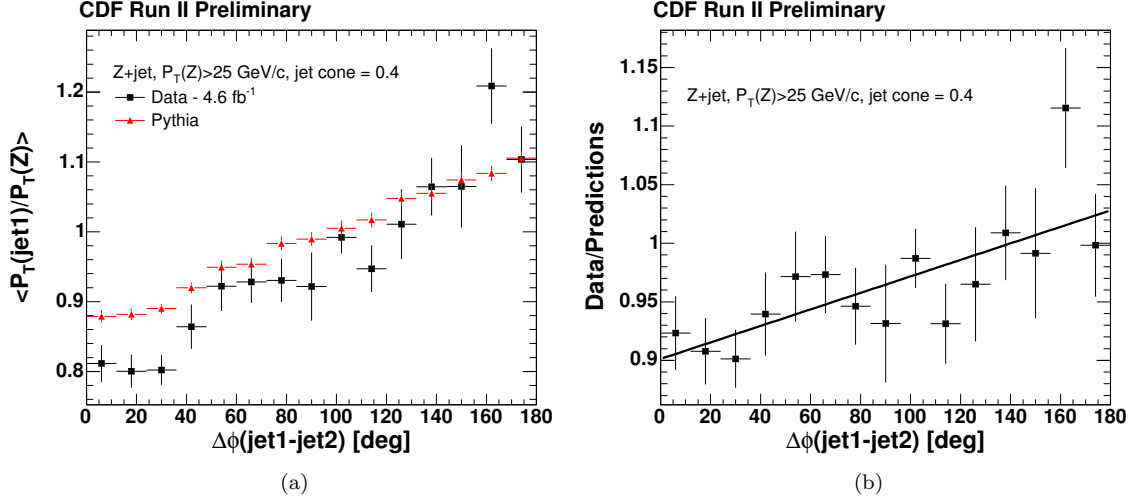


FIG. 13: a.) A comparison of the predicted (triangles) and measured (squares)  $p_T$ -balance as a function of  $\Delta\phi(jet1 - jet2)$  for jets of 0.4 cone size. The predicted balance is obtained with PYTHIA. The events are required to have an only one interaction per event. b.) The fit of the ratio to a line results in  $\chi^2/NDF = 10.0/14$  and slope =  $7.05 \cdot 10^{-4} \pm 1.84 \cdot 10^{-4}$ , as could be explained by an inadequate modeling of large-angle FSR.

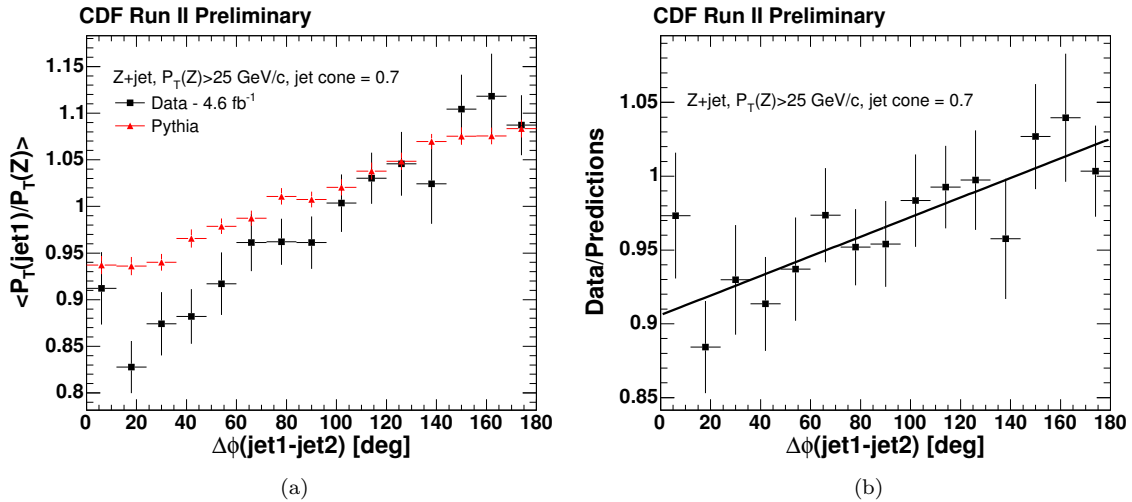


FIG. 14: a.) A comparison of the predicted (triangles) and measured (squares)  $p_T$ -balance as a function of  $\Delta\phi(jet1 - jet2)$  for jets of 0.7 cone size. The predicted balance is obtained with PYTHIA. The events are required to have an only one interaction per event. b.) The fit of the ratio to a line results in  $\chi^2/NDF = 6.9/14$  and slope =  $6.64 \cdot 10^{-4} \pm 1.76 \cdot 10^{-4}$ .

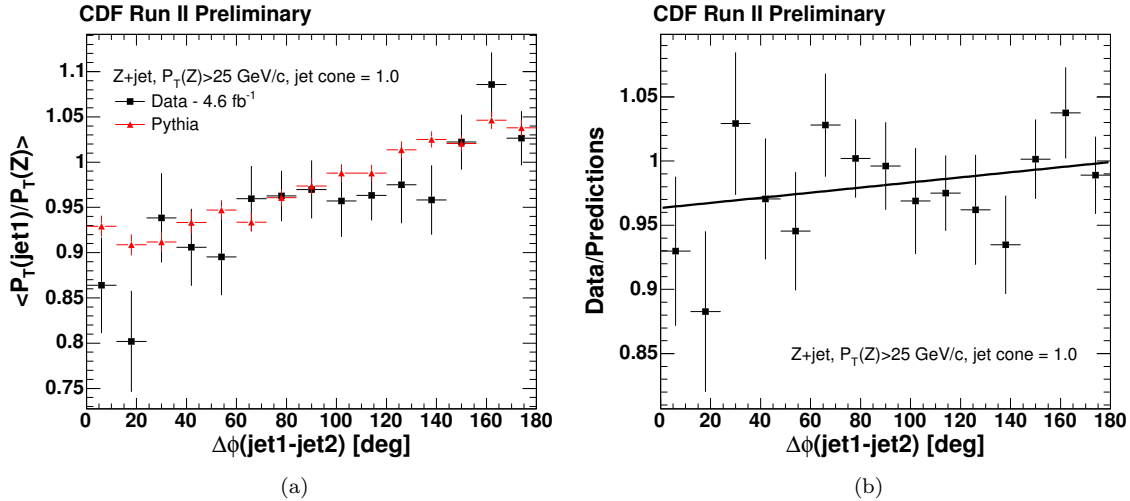


FIG. 15: a.) A comparison of the predicted (triangles) and measured (squares)  $p_T$ -balance as a function of  $\Delta\phi(\text{jet1} - \text{jet2})$  for jets of 1.0 cone size. The predicted balance is obtained with PYTHIA. The events are required to have an only one interaction per event. b.) The fit of the ratio to a line results in  $\chi^2/NDF = 10.5/14$  and slope =  $2.0 \cdot 10^{-4} \pm 2.1 \cdot 10^{-4}$ .

The sensitivity of the  $p_T$ -balance to the separation from the 2nd jet depends on the jet cone size; the disagreement between data and predictions decreases as the jet cone size increases. The trend indicates that the rate of FSR is negatively correlated with the separation from the leading jet. The jet cone size governs splitting and merging of jets so that, for example, two cone-0.4 jets can be reconstructed as one cone-1.0 jet. As a result the large-angle radiation most likely falls within the leading jet cone. The other thing to take into account is that the  $p_T$  cut-off of 8 GeV/c is applied to sub-leading jets of all cone sizes so that the selection is more restrictive for larger jet cone sizes.

Also we study the dependence of the  $p_T$ -balance on the  $p_T$  of the second jet. The balance as a function of the 2nd jet  $p_T$  is shown in Figs. 16, 17, and 18 for different sizes of jet cones. The balance is the most sensitive to the 2nd jet  $p_T$  when the jet cone is 0.4 (see Fig. 16). It is an indication that the rate of large-angle out-of-cone radiation is higher in data than in the predictions.

### A. Uncertainty due to out-of-cone radiation

We use the  $p_T$ -cutoff of the sub-leading jet to estimate the variation of the balance due to the out-of-cone radiation. The agreement between data and predictions improves as we decrease the cut-off value on  $p_T(\text{jet2})$  as shown in Figs. 16, 17, and 18 (all the other selection requirements are kept the same). The extrapolation to the point where  $p_T(\text{jet2})$  is zero describes the case where both data and predictions do not have any large-angle FSR.

We take the variation of the ratio of  $p_T$ -balance between data and predictions as an estimate of the uncertainty due to large angle FSR. The ratio is obtained as a function of  $p_T$  of the sub-leading jet,  $p_T(\text{jet2})$ . The difference between ratios for  $p_T(\text{jet2}) = 0$  GeV/c and  $p_T(\text{jet2}) < 8$  GeV/c is taken as a systematic uncertainty. The obtained uncertainties are summarized in Table III.

### B. Dependence on FSR uncertainties

Final state radiation from unfragmented partons is performed with time-like parton showers in PYTHIA. The predicted  $p_T$ -balance is sensitive to the rate of FSR. The variation of FSR is performed

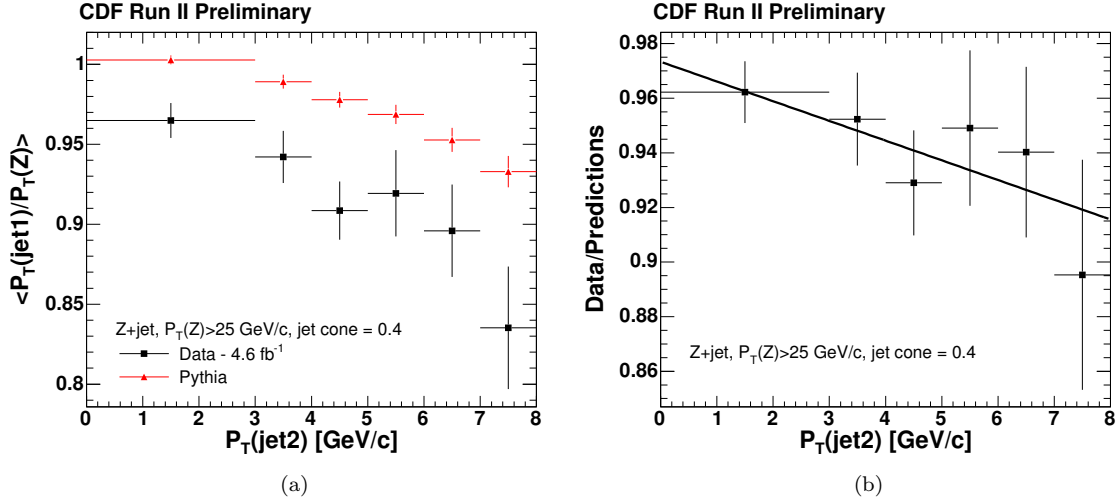


FIG. 16: a.) A comparison of the predicted (triangles) and measured (squares)  $p_T$ -balance as a function of the 2nd jet  $p_T$  for jets of 0.4 cone size. The predicted balance is obtained with PYTHIA. The events are required to have an only one interaction per event. b.) The ratio of predicted to measured  $p_T$ -balance versus the  $p_T$  of the second jet. The linear fit of the ratio resulted with a slope of  $-0.7 \pm 0.4$  %/GeV.

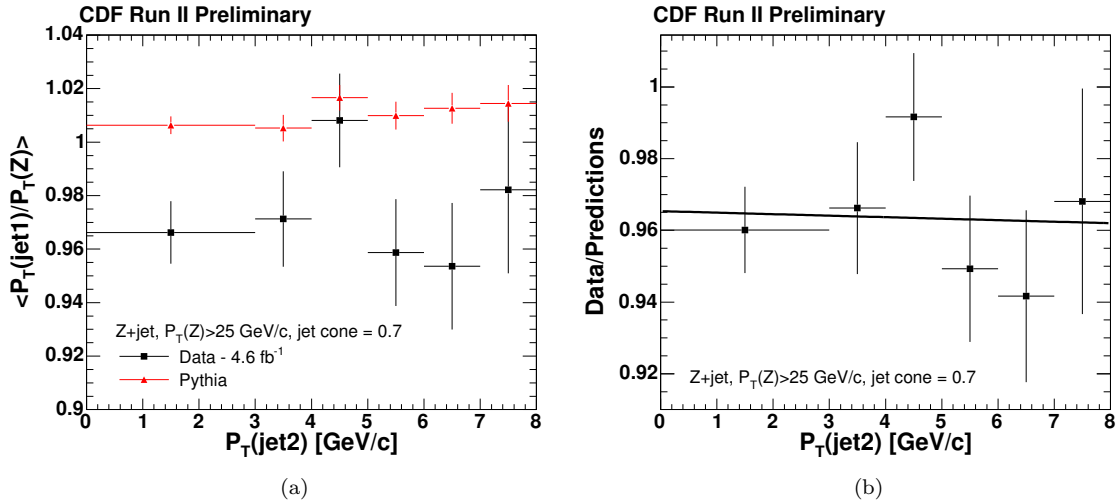


FIG. 17: a.) A comparison of the predicted (triangles) and measured (squares)  $p_T$ -balance as a function of the 2nd jet  $p_T$  for jets of 0.7 cone size. The predicted balance is obtained with PYTHIA. The events are required to have an only one interaction per event. b.) The ratio of predicted to measured  $p_T$ -balance versus the  $p_T$  of the second jet. The linear fit of the ratio resulted with a slope of  $-0.04 \pm 0.04$  %/GeV.

similarly to ISR (see Section VD). To produce the systematics samples we altered the FSR settings used in PYTHIA as it is described in Table I. The value of PARP(72) defines  $\Lambda$  used in simulation of space-like parton showers. The value of PARP(71) is used to multiply the  $Q^2$  scale of the hard scattering to define the maximum parton virtuality for time-like showers. The variation of  $p_T$ -balance

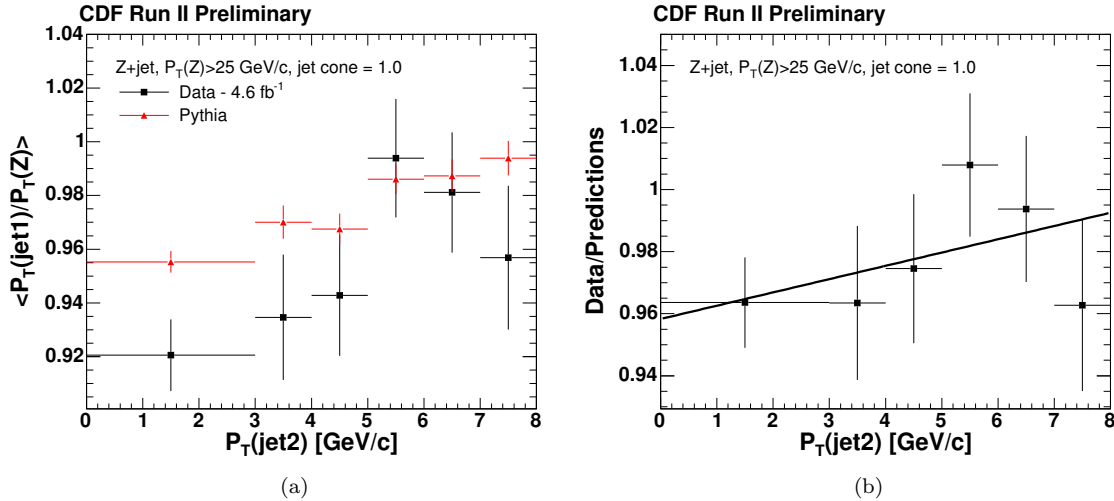


FIG. 18: a.) A comparison of the predicted (triangles) and measured (squares)  $p_T$ -balance as a function of the 2nd jet  $p_T$  for jets of 1.0 cone size. The predicted balance is obtained with PYTHIA. The events are required to have an only one interaction per event. b.) The ratio of predicted to measured  $p_T$ -balance versus the  $p_T$  of the second jet. The linear fit of the ratio resulted with a slope of  $0.4 \pm 0.4$  %/GeV.

in the FSR systematics samples is about 1% and is significantly smaller than the discrepancy between data and predictions.

Sample type	PARP(72), $\text{GeV}/c^2$	PARP(71)
default FSR	0.146	4.0
more FSR	0.292	8.0
less FSR	0.073	2.0

TABLE II: PYTHIA settings used to generate the samples for studies of the systematic uncertainties due to FSR. The input parameter MSTP(3) was set to 1 before providing these to the event generator.

## VII. SYSTEMATIC UNCERTAINTIES ON PREDICTED $p_T$ -BALANCE

We compare the observed discrepancy in  $p_T$ -balance to the predicted uncertainties, some of which we have evaluated earlier. The predicted uncertainties can be divided into three classes:

- Computation-related uncertainties (e.g. choices of  $Q^2$  scale, parametrization of PDF's, underlying event, etc) that can be evaluated by altering parameters in a SM event generator.
- Model-related uncertainties (e.g. those due to the parton-showering) that have to be evaluated by comparing data to SM predictions. The majority of SM event generators do not have higher-order corrections to leading-log parton showering.
- Detector simulation uncertainty affects the predicted jet energy through discrepancies in single-particle response.

The estimated uncertainties are specific to the environment of CDF. The event selection, detector setup, and collisions are different at the LHC experiments. The approaches we provide are meant to

be used as a guideline to improve the jet energy measurements (e.g. JES, top mass,  $\cancel{E}_T$ ) at the LHC experiments.

In this section we evaluate the uncertainties we have not addressed earlier in the paper in order to compare the total uncertainty with the observed discrepancy in the  $p_T$ -balance.

### A. Angular resolution of jets

One would expect that the sensitivity of the  $p_T$ -balance to measurement errors in the direction of the jet should be small, as it is a  $\cos(\phi)$ -effect. The ratio of predicted to measured in fact is consistent with being flat, as expected.

### B. Multiple proton-proton interactions

The  $p_T$ -balance is sensitive to multiple proton-proton interactions overlapping in-time with the hard process (“pile-up”). The number of interactions per event is estimated by observing additional primary vertices along the beam-line. The additional interactions are likely to be minimum-bias collisions.

The uncertainty in the  $p_T$ -balance arises from the present limited ability to measure accurately the calorimeter energy in a minimum bias event. The momentum distribution of charged particles in the predictions, measured in the magnetic spectrometer, was tuned to data for particles with  $p_T > 0.5$  GeV/ $c$  [17]. Soft charged particles ( $p_T < 0.3$  GeV/ $c$ ) curl up in the magnetic field and do not reach the calorimeters. However, all the neutral particles, which always reach the calorimeter, have not been studied. The difference between predictions and data, on the order of a percent, is taken as a systematic uncertainty (see Table III).

### C. Predictions for single particle response

The jet-energy-scale is based on measurements of the single-particle response of the calorimeters to charged particles whose momenta are measured precisely in the magnetic spectrometer of CDF as well as test-beam measurements at the highest momenta [3]. Uncertainties in transferring the measured single-particle response to a parametric model of the calorimeter jet response contribute significantly to the uncertainty on the CDF jet-energy-scale. The contributions are typically several percent (see Table III). We varied the single particle response in a predicted sample by  $\pm 1\sigma$  to estimate its effect on the  $p_T$ -balance.

### D. Summary of systematic uncertainties

We observe a significant discrepancy in the  $p_T$ -balance of  $Z$ -bosons and single jets between measurements and predictions. In Table III we summarize the estimated variations (taken as systematic uncertainties) of the predicted balance. The totality of the variations is comparable to the observed discrepancy, with the largest contributions being from large-angle FSR and the modeling of the single-particle response of the calorimeters.

## VIII. CONCLUSIONS

The official determination of the jet-energy scale, JES, used in Run II CDF analysis was a state-of-art measurement performed with about  $300 \text{ pb}^{-1}$  of data. The overall uncertainty on the JES was taken from  $p_T$ -balance observed in a photon-jet sample.

Source of uncertainty	jet cone = 0.4	jet cone = 0.7	jet cone = 1.0
renormalization and factorization scales	+0.9 -0.0	+0.9 -0.4	$\pm 0.4$
FSR parameters in PYTHIA	$\pm 0.4$	$\pm 0.1$	$\pm 0.1$
ME's and parton-jet matching	+0.8 -0.0	+1.1 -0.0	+0.8 -0.0
single particle response	$\pm 2.5$	$\pm 2.5$	$\pm 2.5$
multiple proton interactions	+1.0 -0.0	+1.2 -0.0	+1.2 -0.0
large-angle FSR, limitation of PS	+0.0 -2.9	+0.0 -0.2	+1.7 -0.0
Estimate of the total variation	+3.0 -3.8	+3.1 -2.5	+3.4 -2.5
The observed discrepancy	+4.7	+3.2	+2.0

TABLE III: The effect on the predicted mean  $p_T$ -balance of varying parameters in the modeling and event selection, in percent. The variations are evaluated for PYTHIA events with  $p_T(Z) > 25$  GeV/ $c$ .

The observed discrepancy is defined as the  $p_T$ -balance in predictions divided by that in data; the predicted jet energies are higher than those in data. The discrepancy between data and predictions is comparable with the estimate of the total variation of the predictions. A positive variation in the predicted  $p_T$ -balance corresponds to an increase in the jet energies in the MC predictions. The total variation is calculated by adding the uncertainties in quadrature.

With significantly more data ( $4.62 \text{ fb}^{-1}$ ) we investigate ways to reduce the systematic uncertainty on jet energy measurements using the  $p_T$ -balance in events with a  $Z$  boson and a jet. We disentangle different effects contributing to the total uncertainty of the JES to investigate the sources of uncertainties. To ensure completeness we compare the sum of the uncertainties to the disagreement observed between the SM predictions and data.

We estimate the sensitivity of the predicted  $p_T$ -balance on parton showering, tree-level matrix elements, parton distribution functions, parton-jet matching procedure, renormalization and factorization scales, multiple  $p\bar{p}$  interactions, and calorimeter response of single stable particles. The contribution from each source of uncertainty is presented in Table III. The uncertainty caused by mis-modeling of the parton shower at large angles is found to be the largest. The sum of the uncertainties is consistent with the discrepancy between data and predictions in the  $p_T$ -balance. The remaining uncertainties (e.g. modeling of Underlying Event, calorimeter stability, etc) are significantly smaller [3] than the discrepancy and we omit them.

The discovery potential of the LHC experiments (ATLAS and CMS) crucially depends on the accuracy of measurements involving hadronic jets with jet and di-jet spectra, the calculation of  $\cancel{E}_T$ , top quark mass, background estimates for BSM searches being prominent examples. The contribution from the each source of uncertainty may vary depending on event selection and detector setup of a given experiment. However, in all cases the accuracy of jet energy measurements can be dramatically improved by developing new models for parton showering, which can describe FSR at large angles, or jet-parton matching schemes.

### Acknowledgments

We thank the Fermilab staff and the technical staffs of the participating institutions for their vital contributions. This work was supported by the U.S. Department of Energy and National Science Foundation; the Italian Istituto Nazionale di Fisica Nucleare; the Ministry of Education, Culture, Sports, Science and Technology of Japan; the Natural Sciences and Engineering Research Council of Canada; the National Science Council of the Republic of China; the Swiss National Science Foundation; the A.P. Sloan Foundation; the Bundesministerium für Bildung und Forschung, Germany; the World Class University Program, the National Research Foundation of Korea; the Science and Technology Facilities Council and the Royal Society, UK; the Institut National de Physique Nucleaire et Physique des Particules/CNRS; the Russian Foundation for Basic Research; the Ministerio de Ciencia e Innovación, and Programa Consolider-Ingenio 2010, Spain; the Slovak R&D Agency; and the Academy of Finland.

We are thankful to David Mietlicki, Ray Culbertson, Peter Skands, Torbjorn Sjostrand, Alexander

Pronko, Larry Nodulman, Willis Sakumoto, Michelangelo Mangano, Christina Mesropian, and Jan-Christopher Winter for suggestions.

This work has been supported by the Maria Goeppert Meyer Fellowship of Argonne National Laboratory, NSF, and DOE.

- 
- [1] B. Meirose. Determination of QCD Backgrounds in ATLAS: A challenge for SUSY searches. 2009.
- [2] Richard Wigmans. Sampling calorimetry. *Nuclear Instruments and Methods in Physics Research Section A: Accelerators, Spectrometers, Detectors and Associated Equipment*, 494(1-3):277 – 287, 2002.
- [3] A. Bhatti et al. Determination of the jet energy scale at the collider detector at fermilab. *Nucl. Instrum. Meth. A*, 566:375–412, 2006.
- [4] B. Abbott et al. Determination of the absolute jet energy scale in the DØ calorimeters. *Nucl. Instrum. Meth.*, A424:352–394, 1999.
- [5] T. Aaltonen et al. Measurement of the  $k_T$  Distribution of Particles in Jets Produced in  $p\bar{p}$  Collisions at  $\sqrt{s} = 1.96$ -TeV. *Phys. Rev. Lett.*, 102:232002, 2009.
- [6] D. Acosta, T. Affolder, H. Akimoto, et al. Momentum distribution of charged particles in jets in dijet events in  $p\bar{p}$  collisions at  $\sqrt{s}=1.8$  tev and comparisons to perturbative qcd predictions. *Phys. Rev. D*, 68(1):012003, Jul 2003.
- [7] Torbjorn Sjostrand, Leif Lonnblad, and Stephen Mrenna. Pythia 6.2: Physics and manual. 2001.
- [8] Michelangelo L. Mangano, Mauro Moretti, Fulvio Piccinini, Roberto Pittau, and Antonio D. Polosa. Alpgen, a generator for hard multiparton processes in hadronic collisions. *JHEP*, 0307:001, 2003.
- [9] Michelangelo L. Mangano, Mauro Moretti, Fulvio Piccinini, and Michele Treccani. Matching matrix elements and shower evolution for top-quark production in hadronic collisions. *JHEP*, 01:013, 2007.
- [10] Private communications with Michelangelo Mangano.
- [11] Transverse momentum and energy are defined as  $p_T = p \sin \theta$  and  $E_T = E \sin \theta$ , respectively. Missing  $E_T$  ( $\cancel{E}_T$ ) is defined by  $\cancel{E}_T = -\sum_i E_T^i \hat{n}_i$ , where  $i$  is the calorimeter tower number for  $|\eta| < 3.6$  (see Ref. [18]), and  $\hat{n}_i$  is a unit vector perpendicular to the beam axis and pointing at the  $i^{th}$  tower. We correct  $\cancel{E}_T$  for jets, photons, electrons and muons. We define the magnitude  $E_T = |\cancel{E}_T|$ .
- [12] F. Abe et al. Topology of three-jet events in  $p\bar{p}$  collisions at  $\sqrt{s}=1.8$  tev. *Phys. Rev. D*, 45(5):1448–1458, Mar 1992.
- [13] Rick Field. Jet physics and the underlying event at the Tevatron. *AIP Conf. Proc.*, 828:163–174, 2006. We use Tune A.
- [14] We use Version 2.10 of ALPGEN.
- [15] PYTHIA v6.216 with a  $M(\gamma^*/Z) > 30$  GeV cut, Tune A, and the “Willis Sakumoto” corrections applied [19]. The  $Z + \text{HF}$  samples are produced with ALPGEN v2.10-prime (which has built-in MLM matching [9]) and showered with PYTHIA v 6.326. The both generators used CTEQ5L parametrization of the parton distribution functions.
- [16] T. Aaltonen et al. Measurement of Cross Sections for  $b$  Jet Production in Events with a  $Z$  Boson in  $p^-$  anti- $p$  Collisions at  $\sqrt{s} = 1.96$ -TeV. *Phys. Rev.*, D79:052008, 2009.
- [17] T. Affolder, H. Akimoto, A. Akopian, et al. Charged jet evolution and the underlying event in proton-antiproton collisions at 1.8 tev. *Phys. Rev. D*, 65(9):092002, Apr 2002.
- [18] The CDF coordinate system is cylindrical and right-handed, with the  $x$  axis horizontal and out of the Tevatron ring, the  $y$  axis up, the  $z$  axis along the proton beam, and  $r = \sqrt{x^2 + y^2}$ ;  $\phi$  is the azimuthal angle. The pseudorapidity  $\eta \equiv -\ln(\tan(\theta/2))$ , where  $\theta$  is the polar angle; the  $\eta$  regions for detector components are defined with respect to the center of the detector. The central region is defined as  $|\eta| < 1$ .
- [19] D. Acosta et al. First measurements of inclusive  $w$  and  $z$  cross sections from run ii of the tevatron collider. *Phys. Rev. Lett.*, 94:091803, 2005.
- [20] The CDF-II detector is described in more detail in many recent publications; see, for example, A. Abulencia et al., (CDF Collaboration), *Phys. Rev. D* **73**, 112006 (2006), and references therein.
- [21] A. Sill et al., *Nucl. Instrum. Meth. A* **447**, 1 (2000); A. Affolder et al., *Nucl. Instrum. Meth. A* **453**, 84 (2000); C.S. Hill, *Nucl. Instrum. Meth. A* **530**, 1 (2000).
- [22] A. Affolder et al., *Nucl. Instrum. Meth. A* **526**, 249 (2004).
- [23] T. Aaltonen et al. First run ii measurement of the  $w$  boson mass at the fermilab tevatron. *Phys. Rev. D*, 77(11):112001, 2008.
- [24] L. Balka et al., *Nucl. Instrum. Meth. A* **267**, 272 (1988).
- [25] S. Kuhlmann et al., *Nucl. Instrum. Meth. A* **518**, 39 (2004).

- [26] D. Acosta et al. (CDF Collaboration), Phys. Rev. D **71**, 032001 (2005).
- [27] M. G. Albrow et al. (CDF Collaboration), Nucl. Instrum. Meth. A **480**, 524 (2002).
- [28] F. Abe et al., Phys. Rev. Lett. **68**, 1104 (1992).
- [29] G. Ascoli et al. (CDF Collaboration), Nucl. Instrum. Meth. A **268**, 33 (1988).
- [30] T. Dorigo et al. (CDF Collaboration), Nucl. Instrum. Meth. A **461**, 560 (2001).
- [31] D. Acosta et al. (CDF Collaboration), Nucl. Instrum. Meth. A **494**, 57 (2002).
- [32] A. Abulencia et al. Measurements of Inclusive W and Z Cross Sections in p-pbar Collisions at  $\sqrt{s}=1.96$  TeV. *J. Phys.*, G34:2457–2544, 2007.
- [33] For central electrons at least 5 hits in each of 3 axial and 2 stereo layers of the COT are required.
- [34] The fraction of electromagnetic energy allowed to leak into the hadron compartment  $E_{\text{had}}/E_{\text{em}}$  must be less than  $0.055+0.00045 \times E_{\text{em}}(\text{GeV})$  for central electrons, less than 0.05 for electrons in the end-plug calorimeters, less than  $\max[0.125, 0.055+0.00045 \times E_{\text{em}}(\text{GeV})]$  for photons.
- [35] D. Acosta et al. (CDF Collaboration), Phys. Rev. D **71**, 051104 (2005); hep-ex/0501023.
- [36] For tight muons at least 5 hits in each of 3 axial and 3 stereo layers of the COT are required; for loose muons with a matching muon stub this is relaxed to 3 axial and 2 stereo. Loose muons without a matching stub have an additional cut on the  $\chi^2$  for the fit to the track.
- [37] The energy deposited in the calorimeter tower traversed by the muon must be less than  $2+\max(0, 0.0115 \times (p-100))$  GeV in the electromagnetic compartment and less than  $6 + \max(0, 0.028 \times (p-100))$  GeV in the hadronic compartment.
- [38] A. V. Varganov. *The Production Cross Sections of the Weak Vector Bosons in Proton Antiproton Collisions at  $\sqrt{s} = 1.96$  TeV and a Measurement of the W Boson Decay Width.* . PhD thesis, University of Michigan, 2004. FERMLAB-THESIS-2004-39.
- [39] The muon “stub” in the muon systems must be within 7, 5, and 6 cm of the extrapolated COT track position, in the CMU, CMP, and CMX muon systems, respectively.
- [40] A. V. Kotwal, H. K. Gerberich, and C.Hays. Identification of cosmic rays using drift chamber hit timing. *Nucl. Instrum. Meth. A*, 506(1-2):110 – 118, 2003.
- [41] The maximum correction to the identification efficiency for central electrons is 1.7%, for “plug” electrons 6.3%, and for central muons is 7.4%.
- [42] T. Aaltonen, A. Abulencia, J. Adelman, et al. First run ii measurement of the  $w$  boson mass at the fermilab tevatron. *Phys. Rev. D*, 77(11):112001, Jun 2008.
- [43] The effective value of  $\Lambda$  used in ISR is  $\Lambda/\sqrt{PARP(64)}$ . Thus, in Table I, the effective value of  $\Lambda$  for the systematic named “more ISR” is  $0.292x\sqrt{2} = 0.413 \text{ GeV}/c^2$  and for “less ISR” it is  $0.073/\sqrt{2} = 0.052 \text{ GeV}/c^2$ . The effective value of  $\Lambda$  corresponds approximately to a cutoff on the allowed  $p_T$  of emissions. The joint use of PARP(61) and PARP(64) results in a more conservative systematic variation than intended.
- [44]  $Q_0 = \sqrt{M_Z^2 + \Sigma p_T^2(jet)}$
- [45] ktfac is a multiplier for  $k_{\perp}$ -measure, which is used to determine the scale for  $\alpha_s$  at each vertex.

## APPENDIX A: THE CDF II DETECTOR

The CDF II detector is a cylindrically symmetric spectrometer designed to study  $p\bar{p}$  collisions at the Fermilab Tevatron. The detector has been extensively described in the literature [20]. Here we briefly describe the detector subsystems relevant for the analysis.

Tracking systems are used to measure the momenta of charged particles, and to trigger on and identify leptons with large transverse momentum,  $p_T$  [11]. A multi-layer system of silicon strip detectors [21], which identifies tracks in both the  $r-\phi$  and  $r-z$  views [18], and the central outer tracker (COT) [22] are contained in a superconducting solenoid that generates a magnetic field of 1.4 T. The COT is a 3.1 m long open-cell drift chamber that makes up to 96 measurements along the track of each charged particle in the region  $|\eta| < 1$ . Sense wires are arranged in 8 alternating axial and stereo ( $\pm 2^\circ$ ) super-layers with 12 wires each. For high momentum tracks, the COT  $p_T$  resolution is  $\sigma_{p_T}/p_T^2 \simeq 0.0017 \text{ (GeV}/c)^{-1}$  [23].

Segmented calorimeters with towers arranged in a projective geometry, each tower consisting of an electromagnetic and a hadronic compartment [24, 25], cover the central region,  $|\eta| < 1$  (CEM/CHA), and the ‘end plug’ region,  $1 < |\eta| < 3.6$  (PEM/PHA). In both the central and end plug regions, systems with finer spatial resolution are used to make profile measurements of electromagnetic showers at shower maximum [26] for electron identification (the CES and PES systems, respectively). Electrons

are reconstructed in the CEM with an  $E_T$  [11] resolution of  $\sigma(E_T)/E_T \simeq 13.5\%/\sqrt{E_T/\text{GeV}} \oplus 2\%$  [24] and in the PEM with an  $E_T$  resolution of  $\sigma(E_T)/E_T \simeq 16.0\%/\sqrt{E_T/\text{GeV}} \oplus 1\%$  [27]. Jets are identified using a cone clustering algorithm in  $\eta-\phi$  space of radius 0.4 as a group of electromagnetic and hadronic calorimeter towers; the jet energy resolution is approximately  $\sigma \simeq 0.1 \cdot E_T(\text{GeV}) + 1.0 \text{ GeV}$  [28].

Muons are identified using the central CMU, CMP, and CMX [29, 30] muon systems, which cover the kinematic region  $|\eta| < 1$ . The CMU system uses four layers of planar drift chambers to detect muons with  $p_T > 1.4 \text{ GeV}/c$  in the central region of  $|\eta| < 0.6$ . The CMP system consists of an additional four layers of planar drift chambers located behind 0.6 m of steel outside the magnetic return yoke, and detects muons with  $p_T > 2.0 \text{ GeV}/c$ . The CMX detects muons in the region  $0.6 < |\eta| < 1.0$  with four to eight layers of drift chambers, depending on the polar angle.

The beam luminosity is measured using two sets of gas Cherenkov counters, located in the region  $3.7 < |\eta| < 4.7$ . The total uncertainty on the luminosity is estimated to be 5.9%, where 4.4% comes from the acceptance and operation of the luminosity monitor and 4.0% from the calculation of the inelastic  $p\bar{p}$  cross-section [31].

A 3-level trigger system [20] selects events for further analysis offline. The first two levels of triggers consist of dedicated fast digital electronics analyzing a subset of the full detector data. The third level, applied to the full data from the detector for those events passing the first two levels, consists of a farm of computers that reconstruct the data and apply selection criteria for (typically) several hundred distinct triggers.

## APPENDIX B: LEPTON IDENTIFICATION

We use standard CDF definitions for identification (ID) of electrons and muons, as described below [32]. The same lepton ID requirements are applied to events from data and Monte Carlo simulations.

The identification and triggering efficiencies for leptons are different for events in data and Monte Carlo, although they demonstrate a very similar energy dependence. To eliminate this inconsistency we follow the standard CDF practice of using correction factors (“scale factors”) to re-weight the MC events (see Section B3).

In order to maintain a high efficiency for  $Z$  bosons, for which we require two identified leptons, we define “tight” and “loose” selection criteria for both electrons and muons, as described below.

To reduce backgrounds from the decays of hadrons produced in jets, leptons are required to be “isolated”. The  $E_T$  deposited in the calorimeter towers in a cone in  $\eta-\varphi$  space [18] of radius  $R = 0.4$  around the lepton position is summed, and the  $E_T$  due to the lepton is subtracted. The remaining  $E_T$  is required to be less than 10% of the lepton  $E_T$  for electrons or  $p_T$  for muons.

### 1. Electron selection

An electron candidate passing the tight selection must be central with  $E_T > 20 \text{ GeV}$ , and have: a) a high quality track [33] with  $p_T > 0.5 \cdot E_T$  or  $p_T > 50 \text{ GeV}/c$ ; b) a good transverse shower profile at shower maximum that matches the extrapolated track position; c) a lateral sharing of energy in the two calorimeter towers containing the electron shower consistent with that expected; and d) minimal leakage into the hadron calorimeter [34].

Additional central electrons, classified as “loose” electrons, are required to satisfy the tight central electron criteria but with a track requirement of  $p_T > 10 \text{ GeV}/c$  (rather than  $0.5 \cdot E_T$ ), and no requirement on a shower maximum measurement or lateral energy sharing between calorimeter towers. Electrons in the end-plug calorimeters ( $1.2 < |\eta| < 2.5$ ), also classified as “loose” electrons, are required to have  $E_T > 20 \text{ GeV}$ , minimal leakage into the hadron calorimeter, a track containing at least 3 hits in the silicon tracking system, and a shower transverse shape consistent with that expected, with a centroid close to the extrapolated position of the track [35].

## 2. Muon selection

A muon candidate passing the tight cuts must have: a) a well measured track in the COT [36] with  $p_T > 20$  GeV/ $c$ ; b) energy deposited in the calorimeter consistent with expectations [37]; c) a muon “stub” [38] in both the CMU and CMP, or in the CMX, consistent with the extrapolated COT track [39]; and d) a COT track fit consistent with an outgoing particle from a  $p\bar{p}$  collision and not from an incoming cosmic ray [40].

Additional muons, classified as “loose”, are required to have  $p_T > 20$  GeV/ $c$  and to satisfy the same criteria as for tight muons but with relaxed COT track quality requirements. Alternatively, for muons outside the muon system fiducial volume, a loose muon must satisfy the tight muon criteria and an additional more stringent requirement on track quality, but the requirement that there be a matching “stub” in the muon systems is dropped.

## 3. Corrections due to Modeling of Electrons and Muons

Following the standard treatment of lepton efficiencies in CDF, we re-weight Monte Carlo events to take into account the difference between the identification efficiencies measured in leptonic  $Z$  decays and those used in simulation [41]. We then make additional corrections for the difference in trigger efficiencies in simulated events and measured in data. Corrections to trigger efficiencies are typically 4% for trigger electrons, 8% for trigger muons that traverse both the CMU and CMP systems, and 5% for muons in the CMX system. The average weight for  $Z \rightarrow e^+e^-$  events is 0.939; for  $Z \rightarrow \mu^+\mu^-$  events it is 0.891.

We correct the energy of electrons and muons the same way as it was done for the measurement of the  $W$  boson mass [42]. The relative positions of the tracker wires were aligned using cosmic muons. Additional track-level corrections were derived using  $W \rightarrow e\nu$  data to reduce bias between positive and negative particles. The electron energy was corrected in data for effects due to tower position and time (aging).